

# PCCP

Accepted Manuscript



This is an *Accepted Manuscript*, which has been through the Royal Society of Chemistry peer review process and has been accepted for publication.

*Accepted Manuscripts* are published online shortly after acceptance, before technical editing, formatting and proof reading. Using this free service, authors can make their results available to the community, in citable form, before we publish the edited article. We will replace this *Accepted Manuscript* with the edited and formatted *Advance Article* as soon as it is available.

You can find more information about *Accepted Manuscripts* in the [Information for Authors](#).

Please note that technical editing may introduce minor changes to the text and/or graphics, which may alter content. The journal's standard [Terms & Conditions](#) and the [Ethical guidelines](#) still apply. In no event shall the Royal Society of Chemistry be held responsible for any errors or omissions in this *Accepted Manuscript* or any consequences arising from the use of any information it contains.

# High thermoelectric performance in two-dimensional graphyne sheets predicted by first-principles calculations

Xiaojian Tan,<sup>a</sup> Hezhu Shao,<sup>a</sup> Tianqi Hu,<sup>a</sup> Guoqiang Liu<sup>\*a</sup> Jun Jiang,<sup>a</sup> and Haochuan Jiang<sup>a</sup>

The thermoelectric properties of two-dimensional graphyne sheets are investigated by using first-principles calculation and Boltzmann transport equation method. The electronic structure indicates a semiconducting phase for graphyne, compared with the metallic phase of graphene. Consequently, the obtained Seebeck coefficient and power factor of graphyne are much higher than those of graphene. The calculated phonon mean free path for graphene is 866 nm, which is in good agreement with the experimental value of 775 nm. Meanwhile the phonon mean free path of graphyne is only 60 nm, leading to the two orders lower thermal conductivity than graphene. We show that the low thermal conductivity of graphyne is due to its mixed  $sp/sp^2$  bonding. Our calculations show that the optimized  $ZT$  values of graphyne sheet can reach 5.3 at intermediate temperature by appropriate doping.

## 1 Introduction

As thermoelectric materials can directly convert heat to electricity and vice versa,<sup>1</sup> they have been attracting increasing attentions both from theoretical and technical sides. The conversion efficiency is governed by the dimensionless figure of merit  $ZT=S^2\sigma T/\kappa$ , where  $S$ ,  $\sigma$ ,  $T$  are, respectively, the Seebeck coefficient, the electrical conductivity, and the absolute temperature. The thermal conductivity  $\kappa$  includes electronic ( $\kappa_e$ ) and phonon contributions ( $\kappa_{ph}$ ).<sup>2</sup> To get high  $ZT$  values is usually difficult since the transport coefficients  $S$ ,  $\sigma$ , and  $\kappa$  are coupled with each other. However, it was predicted that these factors could be decoupled in low dimensional systems.<sup>3</sup> As a representative of low-dimensional carbon materials, graphene has drawn widespread interest in many fields. The electron mobility of graphene is up to  $15000\text{ cm}^2\text{V}^{-1}\text{s}^{-1}$ , which is a great advantage to thermoelectric application.<sup>4,5</sup> Unfortunately, graphene has a very high thermal conductivity of  $2500\sim 5000\text{ W/mK}$ ,<sup>6-8</sup> leading a low  $ZT$  values of 0.02.<sup>9</sup>

Graphyne family is a new type of two-dimensional carbon allotrope. Unlike the  $sp^2$  bonded graphene, graphyne contains two kinds of bonds, namely  $sp$  and  $sp^2$ . Recently, large graphyne film has been successfully prepared and it exhibits excellent semiconducting properties.<sup>10</sup> It is conceivable that graphyne may be more suitable for thermoelectric application than the metallic graphene. Indeed, more and more attention has been paid to the electronic, thermal and thermoelectric properties of graphyne. In the aspect of electronic properties, density functional calculations indicated that a band gap is opened in graphyne by the presence of the  $sp$  bonding.<sup>11-13</sup> Shuai *et al.* calculated the intrinsic mobility in graphyne using first-principles calculations, and it was found that the carrier mobility in graphyne is even larger than that in

graphene.<sup>14-17</sup> In the aspect of thermal conductivity, Zhang *et al.*<sup>18</sup> have shown, based their molecular dynamics (MD) simulations, that the thermal conductivity of graphyne is one order of magnitude lower than that of graphene at room temperature. Lu *et al.*<sup>9,19</sup> applied the nonequilibrium Green's function (NEGF) approach to graphyne, and it was found that the thermal conductance of graphyne is 40% of that of graphene. By using the similar method, Ouyang *et al.*<sup>20,21</sup> have shown that the thermal conductance of  $\beta$ - and  $\gamma$ -graphyne nanoribbons are 26% and 40% of that for graphene nanoribbons, respectively. In the aspect of thermoelectric properties, Wang,<sup>9</sup> Ouyang,<sup>21,22</sup> and Sevinçli<sup>23</sup> predicted that the optimized  $ZT$  values of graphyne sheet can be one order higher than that of graphene, mainly owing to the increase of the power factors. Sun *et al.*<sup>24</sup> carried out MD simulations and showed that the lattice thermal conductivity of graphdiyne is  $7.3\text{ W/mK}$  at room temperature, resulting in a  $ZT$  values of 4.8.

In the previous studies, NEGF method at the ballistic limit is employed to investigate the electron and phonon transport properties. It is known that electron-phonon and phonon-phonon interactions are not well treated in the NEGF method.<sup>25</sup> Some important information, such as the electron or phonon mean free path, can neither be extracted from the calculations. Boltzmann transport equation (BTE) coupled with deformation potentials theory (DPT) was applied to calculate the carrier mobility of some carbon materials<sup>14-17,26,27</sup> and this method was proved to be suitable for describing the electron-phonon coupling of graphyne. Meanwhile, an exact numerical solution of phonon BTE has been developed to study the thermal conductivity. This method has been successfully applied in the phonon transport study for two-dimensional materials such as graphene<sup>6,28</sup> and  $\text{WS}_2$ .<sup>29</sup> In this work, we use the BTE method based on first-principles calculations to investigate the electronic, phonon and thermoelectric properties of graphyne. By considering the phonon-phonon scattering, our theoretical calculations find that the

<sup>a</sup>Ningbo Institute of Materials Technology and Engineering, Chinese Academy of Science, Ningbo 315201, China. Fax: +86-574-86688067; Tel: +86-574-86688067; E-mail: liugq@nimte.ac.cn.

thermal conductivity of graphyne is two orders lower than that of graphene, leading to the much higher thermoelectric performance than the previous predictions.

The rest of this paper is organized as follows. Sec. I-I gives the computational details of our theoretical methods. In Sec. III, we discuss the electronic, phonon, and thermoelectric transport properties of  $\gamma$ -graphyne and graphdiyne. A summary of our work is given in Sec. IV.

## 2 Computational details

The calculations of graphyne are performed using a plane-wave pseudopotential formulation<sup>30–32</sup> within the framework of density functional theory (DFT). The generalized gradient approximation (GGA) of Perdew-Burke-Ernzerhof (PBE)<sup>33</sup> is adopted for exchange-correlation energy. Projector-augmented wave (PAW) potentials are used for the carbon atoms and the cutoff energy is set as 400 eV. The Brillouin zone is sampled with  $20 \times 20 \times 1$ ,  $14 \times 14 \times 1$ , and  $12 \times 12 \times 1$  Monkhorst-Pack  $\mathbf{k}$ -meshes including  $\Gamma$ -point for graphene,  $\gamma$ -graphyne and graphdiyne, respectively. A vacuum layer of 10 Å is added along the  $z$  axis for the two-dimensional structures. During the structure optimizations, both the atoms positions and lattice constants are fully relaxed until the magnitude of the force acting the atoms is less than 0.001 eV/Å, which also converge the total energy within 1 meV.

The electronic transport coefficients are obtained from the analysis of band structure calculations by using the BTE<sup>34</sup> method within the rigid band approximation.<sup>35</sup> This semiclassical approach has been successfully applied to a wide range of thermoelectric materials.<sup>36</sup> The kernel is to find the conductivity tensor

$$\sigma_{\alpha\beta}(\varepsilon) = \frac{1}{N} \sum_{\mathbf{ik}} \sigma_{\alpha\beta}(\mathbf{ik}) \frac{\delta(\varepsilon - \varepsilon_{\mathbf{ik}})}{d\varepsilon}, \quad (1)$$

where  $N$  is the number of  $\mathbf{k}$ -points sampled. To get reliable results, a very dense  $\mathbf{k}$  mesh up to 4000 points for graphyne is used in the BTE calculations. The  $\mathbf{k}$ -dependent conductivity tensor  $\sigma_{\alpha\beta}(\mathbf{ik})$  is given as

$$\sigma_{\alpha\beta}(\mathbf{ik}) = e^2 \tau_{\mathbf{ik}} v_{\alpha}(\mathbf{ik}) v_{\beta}(\mathbf{ik}), \quad (2)$$

where  $\tau(\mathbf{ik})$  is the carrier relaxation time, and the group velocity is  $v(\mathbf{ik}) = (\partial \varepsilon_{\mathbf{ik}} / \partial \mathbf{k}) / \hbar$ . The electrical conductivity  $\sigma$ , Seebeck coefficients  $S$ , and electronic thermal conductance  $\kappa_e$  can be calculated by integrating the conductivity tensor<sup>34</sup>

$$\sigma(T, \mu) = \frac{1}{\Omega} \int \sigma(\varepsilon) \left[ -\frac{\partial f_{\mu}(T, \varepsilon)}{\partial \varepsilon} \right] d\varepsilon, \quad (3)$$

$$S(T, \mu) = \frac{1}{eT\sigma\Omega} \int \sigma(\varepsilon)(\varepsilon - \mu) \left[ -\frac{\partial f_{\mu}(T, \varepsilon)}{\partial \varepsilon} \right] d\varepsilon, \quad (4)$$

$$\kappa_e(T, \mu) = \frac{1}{e^2 T \Omega} \int \sigma(\varepsilon)(\varepsilon - \mu)^2 \left[ -\frac{\partial f_{\mu}(T, \varepsilon)}{\partial \varepsilon} \right] d\varepsilon, \quad (5)$$

where  $\mu$  is the chemical potentials,  $f_{\mu}(T, \varepsilon)$  is the equilibrium Fermi-Dirac distribution, and  $\Omega$  is the volume of the unit cell. Usually,  $\Omega$  is defined for three-dimensional systems. As for two-dimensional graphene and graphyne sheets, a layer thickness is required to define the electrical and thermal conductivity. In order to connect to the previous works, this value is conventionally chosen to be  $\delta = 3.4$  Å, which is the separation between graphene layers in graphite.

The carrier relaxation time  $\tau$  in Eq. (2) measures how quickly the carrier can restore the equilibrium state after scattered by phonons. The DPT method proposed by Bardeen and Shockley<sup>37</sup> can be used to describe the electron-phonon scattering in the long-wave limit. In two-dimensional systems like graphyne, the relaxation time is given by<sup>15,38</sup>

$$\tau = \frac{2\hbar^3 C}{3k_B T m^* E_{DP}^2}, \quad (6)$$

where the parameters  $\hbar$ , and  $k_B$  are Plank constant, and Boltzmann constant, respectively. In addition,  $m^*$  is the density of state effective mass,  $C$  is the elastic constant, and  $E_{DP}$  is the deformation potential constant. These three parameters can be readily obtained from first-principles calculations. Note here  $m^*$  contains contributions from  $k_x$  and  $k_y$  directions, and the degeneracy of light and heavy bands needs to be taken into account.

We calculate the phonon thermal conductivity of graphene,  $\gamma$ -graphyne and graphdiyne by solving the linearized BTE numerically as implemented in the ShengBTE code.<sup>39</sup> A temperature gradient across a material results in a heat flow because of the phonon diffusion from hot to cold. However, these phonons undergo scattering in the diffusion process and the phonon distribution  $f_{qs}$  is changed, where  $s$  is the branch index and  $\mathbf{q}$  is wave vector. The phonon distribution is affected by two factors: diffusion from temperature gradient and scattering due to the allowed processes. In the steady state, the rate of change in the phonon distribution is vanished and it can be expressed by the BTE:<sup>39</sup>

$$\frac{df_{qs}}{dt} = \frac{\partial f_{qs}}{\partial t} \Big|_{diffusion} + \frac{\partial f_{qs}}{\partial t} \Big|_{scattering} = 0, \quad (7)$$

where  $\frac{\partial f_{qs}}{\partial t} \Big|_{diffusion} = -\nabla T \cdot v_{qs} \frac{\partial f_{qs}}{\partial T}$  and  $\frac{\partial f_{qs}}{\partial t} \Big|_{scattering}$  depends on the specific scattering processes, including phonon-phonon scattering, impurities scattering, defects scattering, and so on. Practically, when the only scattering source are the two- and three-phonon scattering processes, a linear version of the BTE is adopted and solved for scattering time  $\tau_{qs}$  by using an iterative method.<sup>39</sup> Finally, the phonon thermal conductivity is given by the formula:<sup>6</sup>

$$\kappa_{ph} = \frac{1}{4\pi^2 \delta k_B T^2} \int (\hbar \omega_{qs})^2 f_{qs} (f_{qs} + 1) v_{qs}^2 \tau_{qs} d\mathbf{q}. \quad (8)$$

Here,  $\omega_{qs}$  and  $v_{qs} = \partial\omega_{qs}/\partial\mathbf{q}$  are the phonon frequency and group velocity, respectively. The  $\delta = 3.4 \text{ \AA}$  is the layer thickness of graphene and graphyne sheets as mentioned before.

Based on the second- and third-order interatomic force constants (IFCs) calculated by first-principles calculations, the phonon dispersions and scattering properties are determined. The results of phonon thermal conductivity are carefully tested with respect to the size of the supercell, the nearest neighboring range, and the  $\mathbf{q}$ -points mesh. In the calculations of second- and third-order IFCs, we use  $10 \times 10 \times 1$  and  $3 \times 3 \times 1$  supercells for graphene and graphyne sheets, respectively. The interactions up to the fourth nearest neighbors are considered when dealing with the anharmonic one. The  $\mathbf{q}$ -points mesh is set as  $100 \times 100 \times 1$ ,  $40 \times 40 \times 1$  and  $30 \times 30 \times 1$  for graphene,  $\gamma$ -graphyne and graphdiyne, respectively.

### 3 Results and discussion

#### 3.1 Crystal and band structure

The structures of two-dimensional  $\gamma$ -graphyne and graphdiyne are illustrated in Fig. 1. These two kinds of graphyne sheets could be considered as benzene rings connected by carbon triplet bonds. The structural symmetry of  $\gamma$ -graphyne and graphdiyne is P6/mmm, as same as graphene. As shown in Fig. 1(b), graphdiyne contains one more acetylenic linkage between the nearest neighboring carbon hexagons than  $\gamma$ -graphyne (Fig. 1(a)). The optimized lattice constants  $a_0$  are 6.890 and 9.460  $\text{\AA}$ . The bond length depicted in Fig. 1 are as follows: for  $\gamma$ -graphyne  $l_1 = 1.426 \text{ \AA}$  ( $sp^2$ - $sp^2$ ),  $l_2 = 1.408 \text{ \AA}$  ( $sp$ - $sp^2$ ), and  $l_3 = 1.223 \text{ \AA}$  ( $sp$ - $sp$ ), and for graphdiyne  $l_1 = 1.432 \text{ \AA}$  ( $sp^2$ - $sp^2$ ),  $l_2 = 1.396 \text{ \AA}$  ( $sp$ - $sp^2$ ), and  $l_3 = 1.233 \text{ \AA}$  ( $sp$ - $sp$ ), and  $l_4 = 1.339 \text{ \AA}$  ( $sp$ - $sp$ ). The obtained structural parameters are in good agreement with the previous LDA<sup>11</sup> and GGA calculations.<sup>12,13,40</sup>

Fig. 2(a-c) presents the calculated energy band structure for graphene,  $\gamma$ -graphyne and graphdiyne. As known, the electronic structure of graphene is characterized by the Dirac cone, where the conduction and valence bands meet at the Dirac point. In  $\gamma$ -graphyne and graphdiyne, the band crossing at the Dirac point is broken due to the presence of  $sp$  bonding, showing a semiconducting behavior. As shown in Fig. 2b and 2c,  $\gamma$ -graphyne has a direct band gap of 0.46 eV at the  $M$  point, and graphdiyne has a direct band gap 0.48 eV at the  $\Gamma$  point. The conduction band maximum (CBM) and valence band minimum (VBM) of  $\gamma$ -graphyne are single degenerate while those of graphdiyne are both double degenerate. The band structures presented in Fig. 2 are consistent with the previous studies.<sup>9,41,42</sup>

Using the formula  $m^* = \hbar^2/(\partial^2 E/\partial\mathbf{k}^2)$ , the effective masses at CBM and VBM can be calculated. As listed in Table 1, the effective masses in  $\gamma$ -graphyne are anisotropic: The

effective masses along the  $\Gamma \rightarrow M$  direction are much larger than those along the  $K \rightarrow M$  direction. In contrast, the effective masses in graphdiyne are rather isotropic. For both  $\gamma$ -graphyne and graphdiyne, there is no significant difference between the hole effective mass and electron one. Narita *et al.*<sup>11</sup> and Kang *et al.*<sup>43</sup> have investigated the band structures and effective masses of  $\gamma$ -graphyne and graphdiyne using local density approximation (LDA) and GGA method. Our calculated results are consistent with their results, as summarized in Table 1. Except for the slightly difference of numerical values, GGA and LDA present similar band gaps and similar effective masses.

#### 3.2 Electronic transport coefficient

Based on the calculated band energies in the first Brillouin zone, the electronic transport coefficients of graphyne can be evaluated by using the semi-empirical BTE approach with the rigid band approximation. Within BTE method, the electrical conductivity  $\sigma$ , electronic thermal conductivity  $\kappa_e$  and power factor  $S^2\sigma$  are calculated with respect to  $\tau$ , that is to say, the obtained electronic transport coefficients are  $\sigma/\tau$ ,  $\kappa_e/\tau$  and  $S^2\sigma/\tau$ . The realistic relaxation time  $\tau$  is energy dependent. However, it is often reasonable to assume a constant  $\tau$  since the electrical conductivity determined by  $\tau$  does not change very much within the energy scale of  $k_B T$ . In this work, the relaxation time is calculated by applying the DPT method with the effective mass approximation.

Besides carrier effective mass, the two other parameters in Eq. (6), elastic constants  $C$  and deformation potential constants  $E_{DP}$ , can also be readily obtained from first-principles calculations. Specifically, we change the lattice constants of graphyne by  $\pm 0.5\%$ ,  $\pm 1.0\%$  and  $\pm 1.5\%$  along the  $a$  and  $b$  axes, and then measure the variation of the total energy and the shift of the VBM and CBM. The two-dimensional elastic constants  $C$  is obtained by fitting the total energy  $E$  with respect to the dilation  $\Delta l/l_0$ , as  $(E - E_0)/S_0 = (C/2)(\Delta l/l_0)^2$ , where  $S_0$  is the cell area in the plane, and  $E_0$  is the total energy at the equilibrium state. The deformation potential constants  $E_{DP}$  for electrons and holes are obtained by fitting the shift CBM and VBM  $\Delta E$  with respect to the dilation, as  $E_{DP} = \Delta E/(\Delta l/l_0)$ . Using the obtained effective mass, elastic constants and deformation potential constants, the relaxation time can be calculated according to Eq. (6).

The calculated relaxation time at room temperature as well as two-dimensional elastic constants, deformation potential constants for  $\gamma$ -graphyne and graphdiyne are summarized in Table 2. Shuai's group has investigated the carriers relaxation time in carbon nanomaterials including graphyne.<sup>14-17</sup> Our calculated results are very consistent with their calculations, as shown in Table 2. It is found that the relaxation times for electrons are longer than those for holes both in  $\gamma$ -graphyne

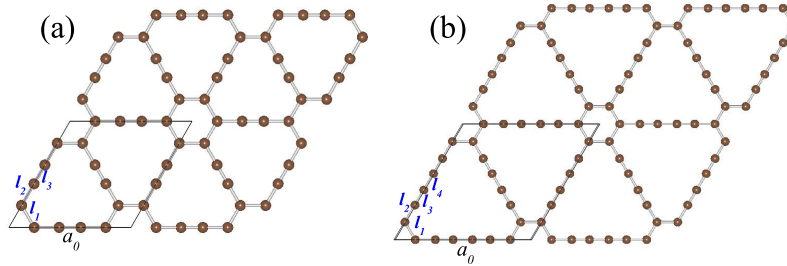


**Fig. 1** (Color online) The structure of (a)  $\gamma$ -graphyne and (b) graphdiyne. The rhombus drawn with a solid line represents a unit cell.

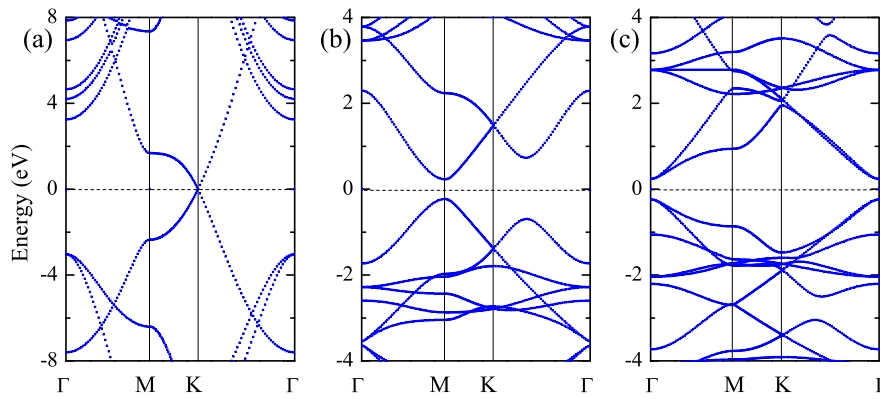


**Fig. 2** (Color online) Calculated band structure of (a) graphene, (b)  $\gamma$ -graphyne, and (c) graphdiyne. The Fermi level is at 0 eV.

**Table 1** The band gap  $E_g$  and effective mass in the conduction band ( $m_c^*$ ) and valence band ( $m_v^*$ ) for  $\gamma$ -graphyne and graphdiyne.

Structure	$E_g$ (eV)	$m_c^*/m_0$		$m_v^*/m_0$	
$\gamma$ -graphyne	0.46 at M	0.197 ( $\Gamma \rightarrow M$ )	0.082 ( $M \leftarrow K$ )	0.215 ( $\Gamma \rightarrow M$ )	0.085 ( $M \leftarrow K$ )
Ref. <sup>11</sup>	0.52 at M	0.15	0.063	0.17	0.066
Ref. <sup>43</sup>	0.46 at M	0.20	0.080	0.21	0.083
graphdiyne	0.48 at $\Gamma$	0.088 ( $M \rightarrow \Gamma$ )	0.090 ( $\Gamma \leftarrow K$ )	0.089 ( $M \rightarrow \Gamma$ )	0.097 ( $\Gamma \leftarrow K$ )
Ref. <sup>11</sup>	0.53 at $\Gamma$	0.073		0.075	

and graphdiyne. As known, the deformation potential constant characterizes the strength of charge-phonon coupling, and weaker charge-phonon coupling leads to longer carrier relaxation times. The calculated  $E_{DP}$  and  $\tau$  suggest that  $n$ -type doping may bring better thermoelectric performance than  $p$ -type doping in the two kinds of graphyne sheets.

According to Eq. (2-5), the electrical conductivity  $\sigma$ , electronic thermal conductivity  $\kappa_e$  and power factor  $S^2\sigma$  are calculated with respect to the electron relaxation time  $\tau$ . As shown in Eq. (6), carrier relaxation times of two-dimensional sheet is inversely proportional to temperature. Within this relationship, the temperature-dependent relaxation times are determined based on the room temperature values, as summarized in Table 2. Fig. 3 plots the electronic transport coefficients map as a function of temperature  $T$  and carrier concentration  $n$  for  $\gamma$ -graphyne (the upper panels) and graphdiyne (the lower panels). In Fig. 3 the positive carrier concentration corresponds to  $n$ -type doping while the negative one corresponds to  $p$ -type doping.

It can be seen from Fig. 3(a) that the Seebeck coefficient  $S$  exhibits two obvious peaks near the Fermi level ( $n = 0$ ), and the peaks of graphdiyne are higher than those of  $\gamma$ -graphyne owing to the slightly larger band gap and double-degenerate bands. As for the electrical conductivity  $\sigma$  shown in Fig. 3(b), there is a sharp increase as the increasing doping concentration when temperature is considered as constant. The electrical conductivity  $\sigma$  of  $\gamma$ -graphyne is higher than that of graphdiyne. The obtained  $\sigma$  for  $n$ -type doping is much larger than for  $p$ -type doping, which is consistent with the above discussions about carrier relaxation times. As known, higher  $\sigma$  requires higher carrier concentration whereas higher  $S$  requires lower carrier concentration. Thus an optimized power factor  $S^2\sigma$  requires a certain compromise between  $S$  and  $\sigma$ . As shown in Fig. 3(c), the maximum  $S^2\sigma$  appears at a moderate doping level where neither  $S$  nor  $\sigma$  reaches its maximum. The calculated electronic thermal conductivity (Fig. 3(d)) shows similar behavior to that of electrical conductivity because of the Wiedemann-Franz law.<sup>44</sup> With higher Seebeck coefficient and lower electrical conductivity, graphdiyne exhibits higher power factor  $S^2\sigma$  and lower  $\kappa_e$  than  $\gamma$ -graphyne at same doping levels.

If we focus on the high temperature areas ( $> 450$  K) of Fig. 3(c), we may find that the optimized power factor is decreasing with the increase of temperature when the carrier concentration is considered as constant. In contrast, the electronic thermal conductivity slightly increases with the increase of temperature, as shown in Fig. 3(d). Thus the  $ZT$  values of these two graphyne sheets will reach their maximums near a moderate temperature (400 ~ 900 K). In addition, compared with the power factor, the electronic thermal conductivity of  $\gamma$ -graphyne increases faster with increasing carrier concentration  $10^{19} \sim 10^{20} \text{ cm}^{-3}$ . Such a trend indicates that  $\gamma$ -graphyne and

graphdiyne could be optimized to exhibit highest  $ZT$  values at relative low carrier concentration.

### 3.3 Phonon dispersion relations and density of state

Fig. 4 displays the calculated phonon dispersions for graphene,  $\gamma$ -graphyne and graphdiyne. The gradually changed colors are determined by the group velocity, and the red and blue color stand for large and small group velocity, respectively. In general, our calculated phonon spectrum for graphene is well consistent with the previous experimental measurement and theoretical calculations.<sup>45,46</sup> As shown in Fig. 4(a), the largest acoustic frequencies of graphene are almost as high as  $1200 \text{ cm}^{-1}$ , and the acoustic branches disperse with very high group velocity. Compared with graphene, the two kinds of graphyne sheets exhibit much lower acoustic branches ( $< 300 \text{ cm}^{-1}$ ) and introduce some new optical branches around  $2200 \text{ cm}^{-1}$ . The optical branches between 200 and  $1500 \text{ cm}^{-1}$  are fairly flat. Both  $\gamma$ -graphyne and graphdiyne exhibit lower acoustic group velocity than graphene.

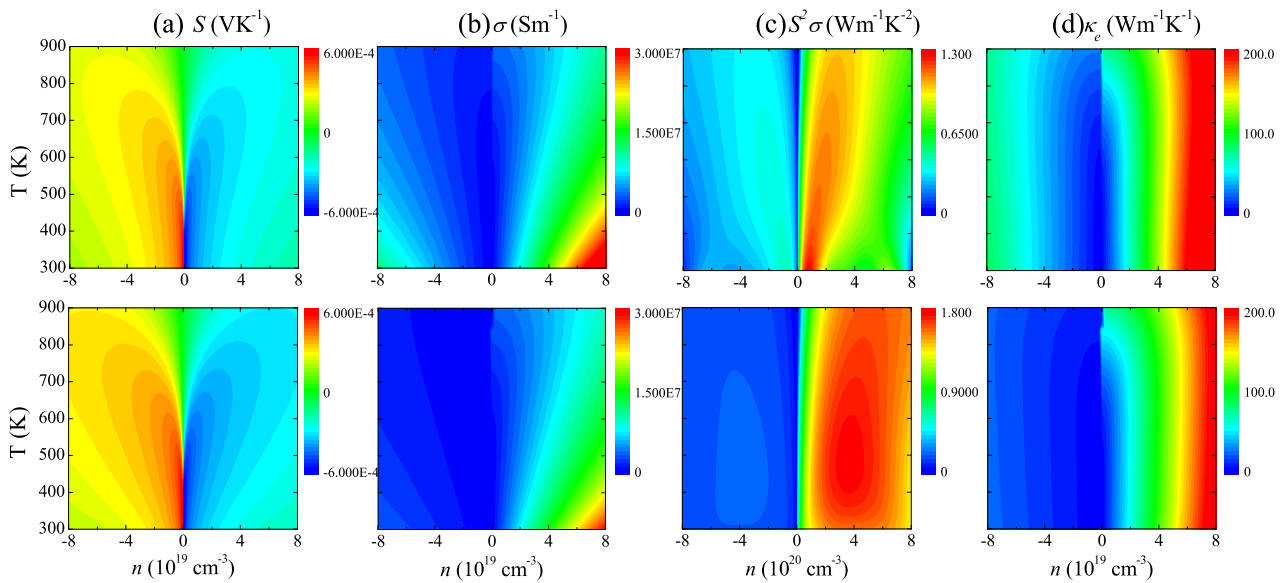
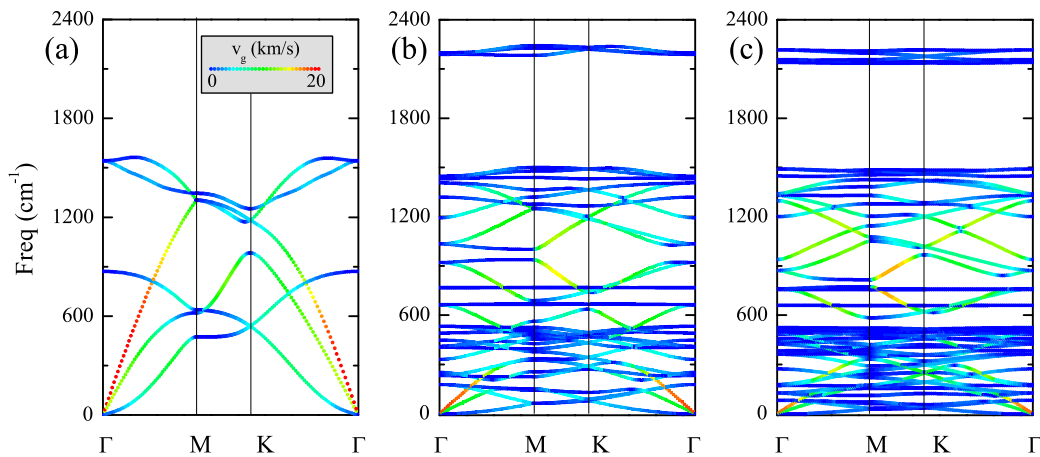
The obtained phonon spectrum of  $\gamma$ -graphyne is well consistent with the previous DFT calculations.<sup>9,20,41</sup> In the case of graphdiyne, the Raman spectra was measured by Li *et al.* They found that the Raman peak at  $1382.2 \text{ cm}^{-1}$  is attributed to the breathing vibration of the  $sp^2$  carbon in aromatic rings while the one at  $2189.8 \text{ cm}^{-1}$  is attributed to the vibration of the  $sp$  carbon in acetylenic linkages.<sup>10</sup> Our calculated phonon spectrum for graphdiyne confirms the observed two phonon branches at  $1339.8 \text{ cm}^{-1}$  and  $2216.5 \text{ cm}^{-1}$ .

Fig. 5(a) presents the phonon density of states (DOS) for graphene,  $\gamma$ -graphyne and graphdiyne. In graphene, the low-frequency ( $< 900 \text{ cm}^{-1}$ ) portion of the phonon DOS is mainly contributed by acoustic phonon. In graphyne, the contribution of acoustic phonon shrinks to a narrow frequency range ( $< 300 \text{ cm}^{-1}$ ). The phonon DOS of graphyne sheets present several peaks at low frequency, showing the decreasing group velocity of acoustic phonon. The intermediate-frequency portion of the phonon DOS are also split into some neighboring peaks, which is consistent with the flat optical branches. The isolated high-frequency DOS around  $2200 \text{ cm}^{-1}$  is consistent with the isolated optical branches.

As mentioned before, graphyne contains  $sp$  and  $sp^2$  hybridized bonds while graphene is all- $sp^2$  bonded. The  $sp$  and  $sp^2$  carbon partial density of states (PDOS) for  $\gamma$ -graphyne and graphdiyne are separated and shown in Fig. 5(b) and (c). It can be seen that the isolated high-frequency phonons ( $2100 \sim 2300 \text{ cm}^{-1}$ ) are completely contributed by  $sp$  carbon atoms, which is very consistent with the previous experimental conclusion.<sup>10</sup> The low-frequency phonons ( $< 600 \text{ cm}^{-1}$ ) are mainly contributed by  $sp$  carbon atoms while the intermediate-frequency branches ( $600 \sim 1500 \text{ cm}^{-1}$ ) are mainly contributed by  $sp^2$  carbon atoms. As shown, the phonon DOS of

**Table 2** Elastic constants  $C$ , deformation potential constants  $E_{DP}$ , and carrier relaxation time  $\tau$  for  $\gamma$ -graphyne and graphdiyne at 300 K.

Structure		axes	$C$ ( $Jm^{-2}$ )	$E_{DP}^h$ (eV)	$E_{DP}^e$ (eV)	$\tau^h$ (ps)	$\tau^e$ (ps)
$\gamma$ -graphyne	Present work	$a$	220.35	4.56	2.81	0.49	1.41
		$b$	220.38	4.57	2.79	0.49	1.43
graphdiyne	Ref <sup>17</sup>					0.56	1.25
						0.21	1.79
	Present work	$a$	167.26	6.99	2.37	0.21	1.79
		$b$	167.25	7.03	2.37	0.22	1.92
Ref <sup>14–16</sup>	$a$	158.57	6.30	2.09			
	$b$	144.90	6.11	2.19			

**Fig. 3** (Color online) Calculated electronic transport coefficients map as a function of temperature  $T$  and carrier concentration  $n$  for  $\gamma$ -graphyne (top) and graphdiyne (bottom).**Fig. 4** (Color online) Calculated phonon dispersion relations for (a) graphene, (b)  $\gamma$ -graphyne and (c) graphdiyne. The gradually changed colors from blue to red indicate the group velocity for the corresponding phonon branches ( $0 \sim 20 \text{ km s}^{-1}$ ).

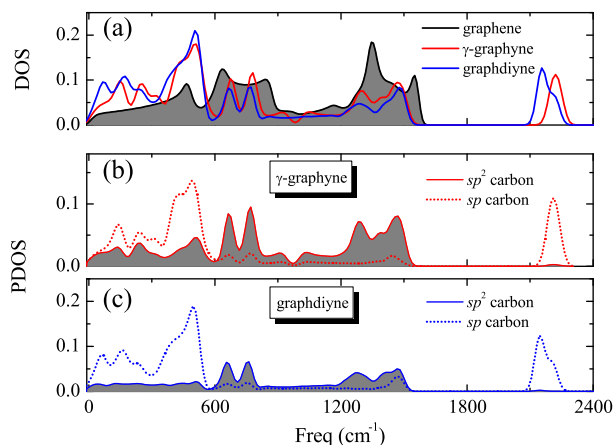


**Fig. 5** (Color online) Calculated phonon density of state (DOS) (a) and the  $sp$ -,  $sp^2$ -carbon partial density of state (PDOS) for (b)  $\gamma$ -graphyne and (c) graphdiyne.

$sp^2$ -hybridized aromatic rings in graphyne almost remain the same shape as in graphene. Along the series of graphene,  $\gamma$ -graphyne, and graphdiyne, the  $sp^2$  component in lower-frequency phonons is gradually replaced by the  $sp$  one. The phonon DOS shows that the presence of the  $sp$  bonding decreases the group velocity of acoustic branches and introduces some new optical branches, implying much lower phonon thermal conductivity in graphyne than in graphene.

### 3.4 Phonon thermal conductivity

As discussed in the introduction, the phonon thermal conductance of graphene and graphyne has been investigated by using the NEGF method within the ballistic limit.<sup>9,19–21,23</sup> The NEGF results show a monotonously increase of phonon thermal conductance with the increasing temperature. In the NEGF method, the phonon transport are treated as ballistic transport, and the phonon-phonon interaction is neglected. This approximate is just applicable at low temperature when phonon scattering is weak. From room temperature to intermediate temperature range, phonon-phonon scattering processes dominate the phonon transport and should be reasonably treated. In this work, the adopted phonon BTE method is applied to handle the phonon scattering effect, and describe the relationship between phonon thermal conductivity and temperature.

Fig. 6 displays the calculated phonon thermal conductivity as a function of temperature for graphene,  $\gamma$ -graphyne and graphdiyne. The  $\kappa_{ph}$  of graphene at room temperature is  $3845 \text{ W m}^{-1} \text{ K}^{-1}$ , which is consistent with the experimental measurement ( $2500 \sim 5000 \text{ W m}^{-1} \text{ K}^{-1}$ <sup>7,8</sup>) and close to the previous theoretical calculations ( $3435 \sim 3800 \text{ W m}^{-1} \text{ K}^{-1}$ <sup>6,47</sup>).

As shown in Fig. 6, our results are roughly scaled by  $\kappa_{ph} \sim 1/T^\alpha$  ( $\alpha=1.66, 0.93$ , and  $0.75$  for graphene,  $\gamma$ -graphyne and graphdiyne, respectively). The decreased thermal conductivity at high temperature can be owed to the more frequent phonon-phonon scattering. The calculated values for these two graphyne sheets are much lower than that of graphene in the whole temperature range. At room temperature, and the thermal conductivities are  $82.3$  and  $22.3 \text{ W m}^{-1} \text{ K}^{-1}$  for  $\gamma$ -graphyne and graphdiyne, respectively. These results are consistent with the above analysis of phonon dispersion and DOS.

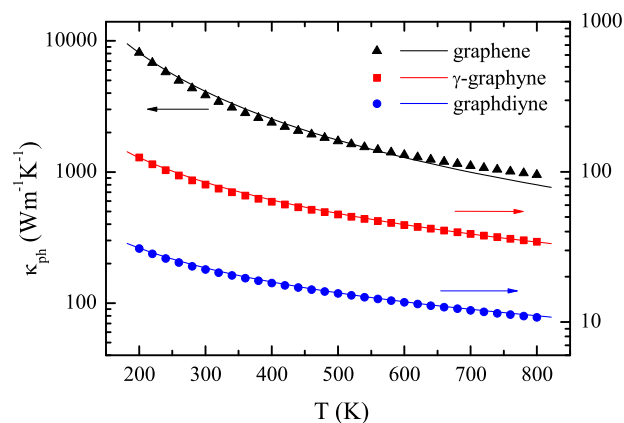


**Fig. 6** (Color online) Calculated phonon thermal conductivity as a function of temperature for graphene,  $\gamma$ -graphyne and graphdiyne. The fitting curves of  $\kappa_{ph} \sim 1/T^\alpha$  are also shown.

In a quantitative comparison, the phonon thermal conductivity of  $\gamma$ -graphyne and graphdiyne are only 3% and 1% of that of their allotrope graphene, respectively. It is meaningful to understand the huge difference of the phonon transport properties between these similar two-dimensional materials. As known, phonon thermal conductivity of two-dimensional sheet can be written as:  $\kappa_{ph} = C_V \bar{v}_g \bar{l} / 2$ , where  $C_V$ ,  $\bar{v}_g$ , and  $\bar{l}$  are the specific heat, group velocity, and phonon mean free path (MFP). In this work, the phonon mean free path  $\bar{l}$  is calculated as the the average of free path over all the phonon modes:

$$\bar{l} = \frac{1}{N_{qs}} \sum_{qs} v_{qs} \tau_{qs}, \quad (9)$$

where  $N_{qs}$  is the number of  $\mathbf{q}$ -points sampled.

The calculated  $C_V$ ,  $\bar{v}_g$ , and  $\bar{l}$  at 300 K for graphene,  $\gamma$ -graphyne and graphdiyne are summarized in Table 3. As shown, there is no obvious difference between the specific heat while the mean group velocity of graphene is almost triple of those of graphyne. Our calculated phonon MFP for graphene is 866 nm, which is very close to the experimental measured value 775 nm.<sup>48</sup> The phonon MFP of  $\gamma$ -graphyne



and graphdiyne are nearly one or two orders shorter than that of graphene. Considering the shorter phonon MFP, the much lower phonon thermal conductivity of graphyne can be understood. The previous NEGF calculations assumed that graphyne and graphene have the same MFP of 775 nm, and their obtained phonon thermal conductance  $\sigma_{ph}$  of graphyne is 60% lower than that of graphene.<sup>9,19–23</sup> Our works show that the mixed  $sp/sp^2$  bonds in graphyne sheet increase phonon-phonon scattering, and the calculated phonon MFP of graphyne is much shorter than that of graphene, resulting in the two orders lower thermal conductivity.

It is interesting to examine the distribution of phonon free paths in graphene,  $\gamma$ -graphyne and graphdiyne. Fig. 7 presents the normalized cumulative phonon thermal conductivity as a function of the free path at 300 K. Their phonon thermal conductivity distribution curves look very similar, except for the different scales of phonon free paths. Usually, low-frequency phonon modes with large free paths dominate in the anharmonic scattering processes, and high-frequency modes with small free paths contribute a little to the thermal conductivity.<sup>49,50</sup> As shown in Fig. 7, the thermal conductivity of graphene is mostly contributed from long free path phonons, and the fraction of heat transport carried by phonon with free paths longer or equal to 1000 nm is  $\sim 55\%$ . The phonon free paths of  $\gamma$ -graphyne distribute in the range of 1  $\sim$  5000 nm, and the longer free path phonons ( $> 100$  nm) nearly contribute half of the thermal conductivity. The free paths of graphdiyne are almost shorter than 1000 nm. Its thermal conductivity is mostly contributed from short free path phonons, and the fraction of heat transport carried by phonon with free path shorter or equal to 20 nm is  $\sim 55\%$ .

### 3.5 Optimized $ZT$ values

With the obtained transport coefficients, we are now able to evaluate the thermoelectric performance of graphyne according to  $ZT = S^2 \sigma T / (\kappa_e + \kappa_{ph})$ . Fig. 8(a) and (b) presents the  $ZT$  value as a function of temperature  $T$  and carrier concentration  $n$  for  $\gamma$ -graphyne and graphdiyne, respectively. The red and blue colors stand for large and small  $ZT$  values, respectively, as shown in the color scale. As can be seen from Fig. 8, the calculated  $ZT$  values exhibit high values in a wide temperature range. This observation suggests that one can always obtain high thermoelectric performance of graphyne by appropriate doping. The  $n$ -type graphyne sheets exhibit larger  $ZT$  values than the  $p$ -type systems, which is mainly caused by relatively higher electrical conductivity and power factor of  $n$ -type doping (see Fig. 3(b) and (c)). In addition, due to the higher power factor (see Fig. 3(c)), lower electronic thermal conductivity (see Fig. 3(d)) and lower phonon thermal conductivity (see Fig. 6), graphdiyne can be doped to exhibit larger  $ZT$  values than  $\gamma$ -graphyne.

The optimized  $ZT$  values of  $\gamma$ -graphyne and graphdiyne at 300 K are summarized in Table 4, where the corresponding carrier concentration  $n$  and transport coefficients  $S$ ,  $\sigma$ ,  $S^2 \sigma$ ,  $\kappa_e$ , and  $\kappa_{ph}$  are also given. Wang *et al.*<sup>9</sup> have reported that the optimized  $ZT$  of graphene at room temperature is 0.0094. The corresponding transport coefficients are extracted from their works and listed in Table 4 for comparison. It is found that graphyne could exhibit higher power factor than graphene by light doping ( $\sim 10^{19} \text{ cm}^{-3}$ ). As shown in the previous reports, the mixed  $sp/sp^2$  bonds open a band gap in graphyne sheet.<sup>11–13</sup> The low electronic thermal conductivity, high Seebeck coefficient and improved power factor in graphyne can be owing to the presence of  $sp$  bonding. On the other hand,  $sp$  bonding in graphyne sheet leads to low thermal conductivity. Reasonably, high  $ZT$  values are obtained in graphyne sheet. Compared with  $\gamma$ -graphyne, graphdiyne contains more  $sp$  bondings, and it exhibits lower thermal conductivity and higher  $ZT$  value.

As shown in Table 4, our calculations indicate that the two orders lower phonon thermal conductivity in graphyne sheets significantly increase the  $ZT$  values. The optimized  $ZT$  value of graphdiyne at room temperature is 0.99 and 3.26 by  $p$ -type and  $n$ -type doping, respectively. These values mostly exceed the previous reports and make graphyne very promising candidate for thermoelectric applications. In the previous studies, Wang *et al.* and Sevinçli *et al.* have independently studied the thermoelectric property of  $\gamma$ -graphyne sheet by using the NEGF method within ballistic approach. They obtained similar results and the optimized  $ZT$  value for  $\gamma$ -graphyne is only about 0.16 at 300 K.<sup>9,23</sup> They attributed the relatively larger  $ZT$  values of graphyne to the larger Seebeck coefficients. The huge difference of phonon mean free path between graphene and graphyne is neglected by the NEGF method, which leads to overestimated thermal conductivity and underestimated  $ZT$  value for graphyne sheet.<sup>9,23</sup> Sun *et al.* have investigated the thermoelectric property of graphdiyne by a combination of BTE method and MD simulation, and the optimized  $ZT$  value for graphdiyne is 4.8 at 300 K.<sup>24</sup> As known, MD results strongly depend on the empirical potential coefficients. It seems that the thermal conductivity of graphene and graphyne by MD method are underestimated compared with experimental values. For example, the MD results show that the lattice thermal conductivity of graphene at 300 K is only 100 W/mK<sup>18</sup>, which is much smaller than the experimental measurement (2500  $\sim$  5000 W/mK)<sup>6,7</sup>. The high  $ZT$  value of 4.8 for graphdiyne reported by Sun may result from the underestimated thermal conductivity (7.3 W/mK at 300 K).

It can be seen from Fig. 8 that  $\gamma$ -graphyne and graphdiyne exhibit very high  $ZT$  values in a wide operating temperature range around 800 K and 600 K, respectively. The highest  $ZT$  values and the corresponding transport coefficients are summarized in Table 4. Compared with the results at room tem-

**Table 3** Calculated specific heat  $C_V$ , mean values of group velocity  $\bar{v}_g$ , phonon mean free path  $\bar{l}$ , and thermal conductivity  $\kappa_{ph}$  for graphene,  $\gamma$ -graphyne and graphdiyne at 300 K.

Structure	$C_V (Jcm^{-3}K^{-1})$	$\bar{v}_g (kms^{-1})$	$\bar{l} (nm)$	$\kappa_{ph} (Wm^{-1}K^{-1})$
graphene	1.64	5.42	866 (775 <sup>48</sup> )	3845
$\gamma$ -graphyne	1.68	1.65	59.5	82.3
graphdiyne	1.47	1.66	18.3	22.3

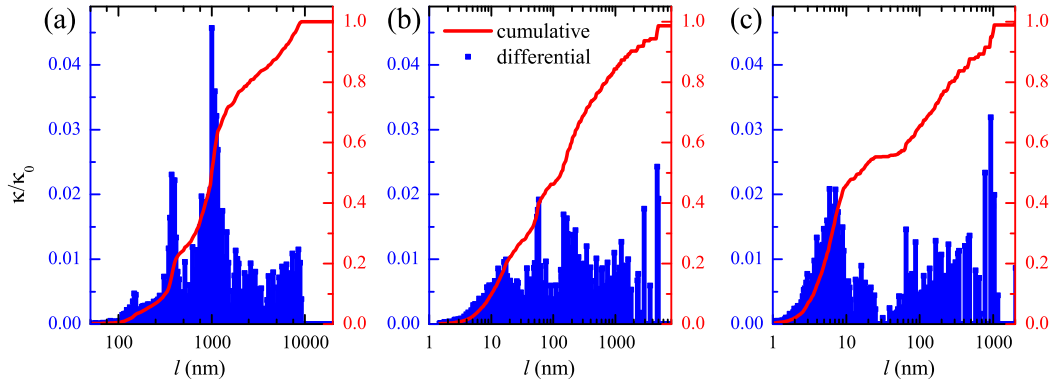


**Fig. 7** (Color online) Normalized cumulative phonon thermal conductivity as a function of the mean free path at 300 K for (a) graphene, (b)  $\gamma$ -graphyne and (c) graphdiyne.

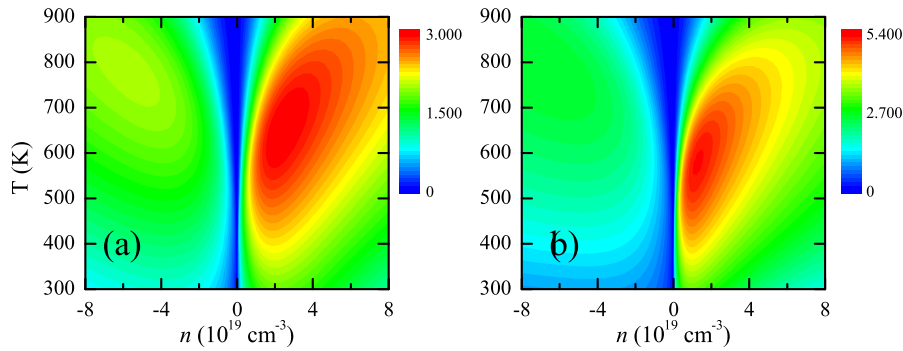


**Fig. 8** (Color online) Calculated  $ZT$  value map as a function of temperature  $T$  and carrier concentration  $n$  for (a)  $\gamma$ -graphyne and (b) graphdiyne.

**Table 4** Optimized  $ZT$  values of  $\gamma$ -graphyne and graphdiyne at 300 K as well as the optimal operating temperature. The corresponding optimal carrier concentration  $n$ , Seebeck coefficient  $S$ , electrical conductivity  $\sigma$ , power factor  $S^2\sigma$ , and the electronic and phonon thermal conductivity  $\kappa_e$  and  $\kappa_{ph}$  are also indicated.

Structure	$n (10^{19}cm^{-3})$	$S (\mu VK^{-1})$	$\sigma (10^6 Sm^{-1})$	$S^2\sigma (Wm^{-1}K^{-2})$	$\kappa_e (Wm^{-1}K^{-1})$	$\kappa_{ph} (Wm^{-1}K^{-1})$	$ZT$
graphene <sup>9</sup>	@300 K	~77	~16.4	~0.097	~130	~2960	0.0094
$\gamma$ -graphyne	-4.0@300 K	260	5.55	0.38	40.8	82.3	0.91
	2.1@300 K	-316	8.96	0.89	65.9	82.3	1.81
	-5.5@780 K	286	2.78	0.23	53.0	34.4	2.02
	3.3@760 K	-307	5.76	0.55	107.2	35.2	2.92
graphdiyne	-4.8@300 K	248	1.91	0.12	14.0	22.3	0.99
	1.1@300 K	-372	4.09	0.57	30.1	22.3	3.26
	-7.0@800 K	315	0.95	0.09	18.7	10.8	2.56
	1.2@580 K	-429	2.34	0.43	33.2	13.8	5.30

perature, the optimized  $ZT$  values increase from 1.81, 3.26 to 2.92, 5.30 for  $n$ -type  $\gamma$ -graphyne and graphdiyne, respectively. The increased  $ZT$  values result from the exponential decline of phonon thermal conductivity and the mild decreasing of power factor. As shown in Table 4, the electronic thermal conductivity is comparable and even excess of the phonon contribution, which is not uncommon in doped systems.<sup>9</sup> We note that the  $ZT$  value of graphdiyne is higher than 3.0 in a very wide temperature range (almost 300 ~ 900 K) and wide doping range ( $n = 0.2 \sim 8.0 \times 10^{19} \text{cm}^{-3}$ ), which implies that this graphdiyne is particularly suitable for fabrication of the thermoelectric modules.

## 4 Summary

In summary, the electronic, thermal, and thermoelectric transport properties of  $\gamma$ -graphyne and graphdiyne are investigated by using first-principles calculation and Boltzmann transport equation method. Graphyne exhibits much higher Seebeck coefficients than graphene, which is consistent with its semiconducting band structure. The deformation theory is adopted to describe the electron-phonon interaction and the our results predict the carrier relaxation times of electron is larger than those of hole, implying better thermoelectric performance in  $n$ -type graphyne. Contrary to the previous NEGF calculations, our calculated lattice thermal conductivity of graphyne is found to be two orders lower than graphene. The phonon spectra and DOS indicate that the low lattice thermal conductivity originates in the decrease of group velocity and the appearance of new phonon branches. The calculated phonon MFPs for graphene,  $\gamma$ -graphyne, and graphdiyne are 866, 60, and 18 nm, respectively. We argue that the overestimate of lattice thermal conductivity in previous studies is due to the rough description of phonon-phonon scattering. With the high power factor and relative low thermal conductivity, graphdiyne possesses superior thermoelectric performance with a maximum  $ZT$  value of 5.3 at 580 K. Our study suggest that major effort should be paid on the realization of these high-performance and environmentally-friendly thermoelectric materials.

This work was supported by the National Natural Science Foundation of China (No. 11404350, 11404348 and 11234012) and Ningbo Science and Technology Innovation Team (No. 2014B82004). All calculations were performed in the PC Cluster from Sugon Company of China.

## References

- 1 L. Bell, *Science*, 2008, **321**, 1457.
- 2 G. A. Slack, In *CRC Handbook of Thermoelectrics*, edited by D. M. Rowe, (CRC Press, Boca Raton FL), 1995, p407.
- 3 L. D. Hicks, and M. S. Dresselhaus, *Phys. Rev. B*, 1993, **47**, 12727.
- 4 S. V. Morozov, K. S. Novoselov, M. I. Katsnelson, F. Schedin, D. C. Elias, J. A. Jaszczak, and A. K. Geim, *Phys. Rev. Lett.*, 2008, **100**, 016602.
- 5 A. H. Castro Neto, F. Guinea, N. M. R. Peres, K. S. Novoselov, and A. K. Geim, *Rev. Mod. Phys.*, 2009, **81**, 109.
- 6 L. Lindsay, D. A. Broido, and N. Mingo, *Phys. Rev. B*, 2010, **82**, 115427.
- 7 A. A. Balandin, *Nat. Mater.*, 2011, **10**, 569.
- 8 D. L. Nika, and A. A. Balandin, *J. Phys.: Condens. Matter*, 2012, **24**, 233203.
- 9 X. M. Wang, D. C. Mo, and S. S. Lu, *J. Chem. Phys.*, 2013, **138**, 204704.
- 10 G. X. Li, Y. L. Li, H. B. Liu, Y. B. Guo, Y. J. Li, and D. B. Zhu, *Chem. Commun.*, 2010, **46**, 3256.
- 11 N. Narita, S. Nagai, S. Suzuki, K. and Nakao, *Phys. Rev. B*, 1998, **58**, 11009.
- 12 J. Zhou, K. Lv, Q. Wang, X. S. Chen, Q. Sun, and P. Jena, *J. Chem. Phys.*, 2011, **134**, 174701.
- 13 L. D. Pan, L. Z. Zhang, B. Q. Song, S. X. Du, and H. J. Gao, *Appl. Phys. Lett.*, 2011, **98**, 173102.
- 14 M. Q. Long, L. Tang, D. Wang, Y. L. Li, and Z. G. Shuai, *ACS Nano*, 2011, **5**, 2593.
- 15 J. Y. Xi, M. Q. Long, L. Tang, D. Wang, and Z. G. Shuai, *Nanoscale*, 2012, **4**, 4348.
- 16 J. M. Chen, J. Y. Xi, D. Wang, and Z. G. Shuai, *J. Phys. Chem. Lett.*, 2013, **4**, 1443.
- 17 J. Y. Xi, D. Wang, Y. P. Yi, and Z. G. Shuai, *J. Chem. Phys.*, 2014, **141**, 034704.
- 18 Y. Y. Zhang, Q. X. Pei, and C. M. Wang, *Comput. Mater. Sci.*, 2012, **65**, 406.
- 19 X. M. Wang, and S. S. Lu, *J. Phys. Chem. C*, 2013, **117**, 19740.
- 20 T. Ouyang, Y. P. Chen, L. M. Liu, Y. E. Xie, X. L. Wei, and J. X. Zhong, *Phys. Rev. B*, 2012, **85**, 235436.
- 21 T. Ouyang, and M. Hu, *Nanotechnology*, 2014, **25**, 245401.
- 22 T. Ouyang, H. P. Xiao, Y. E. Xie, X. L. Wei, Y. P. Chen, and J. X. Zhong, *J. Appl. Phys.*, 2013, **114**, 073710.
- 23 H. Sevinçli, and C. Sevik, *Appl. Phys. Lett.*, 2014, **105**, 223108.
- 24 L. Sun, P. H. Jiang, H. J. Liu, D. D. Fan, J. H. Liang, J. Wei, L. Cheng, J. Zhang, and J. Shi, *Carbon*, 2015, **90**, 255.
- 25 J.-S. Wang, J. Wang, and N. Zeng, *Phys. Rev. B*, 2006, **74**, 033408.
- 26 D. Wang, W. Shi, J. M. Chen, J. Y. Xi, and Z. G. Shuai, *Phys. Chem. Chem. Phys.*, 2012, **14**, 16505.
- 27 J. M. Chen, D. Wang, and Z. G. Shuai, *J. Chem. Theory Comput.*, 2012, **8**, 3338.
- 28 A. Cepellotti, G. Fugallo, L. Paulatto, M. Lazzeri, F. Mauri, and N. Marzari, *Nat. Commu.*, 2015, **6**, 6400.
- 29 A. N. Gandi, and U. Schwingenschlöggl, *Chem. Matter.*, 2014, **26**, 6628.
- 30 G. Kresse, and J. Hafner, *Phys. Rev. B*, 1993, **47**, R558.
- 31 G. Kresse, and J. Hafner, *Phys. Rev. B*, 1994, **49**, 14251.
- 32 G. Kresse, and J. Furthmüller, *Comput. Mater. Sci.*, 1996, **6**, 15.
- 33 J. P. Perdew, K. Burke, and M. Ernzerhof, *Phys. Rev. Lett.*, 1996, **77**, 3865.
- 34 G. K. H. Madsen, and D. J. Singh, *Comput. Phys. Commun.*, 2006, **175**, 67.
- 35 M. G. Holland, *Phys. Rev.*, 1963, **132**, 2461.
- 36 D. J. Singh, *Sci. Adv. Mater.*, 2011, **3**, 561.
- 37 J. Bardeen, and W. Shockley, *Phys. Rev.*, 1950, **80**, 72.
- 38 P. J. Price, *Ann. Phys.*, 1981, **133**, 217.
- 39 W. Li, J. Carrete, N. A. Katcho, and N. Mingo, *Comput. Phys. Commun.*, 2014, **185**, 1747.
- 40 Q. Peng, W. Ji, and S. De, *Phys. Chem. Chem. Phys.*, 2012, **14**, 13385.
- 41 N. K. Perkgoz, and C. Sevik, *Nanotechnology*, 2014, **25**, 185701.
- 42 Y. Jiao, A. J. Du, M. Hankel, Z. H. Zhu, V. Rudolph, and S. C. Smith, *Chem. Commun.*, 2011, **47**, 11843.

- 
- 43 J. Kang, J. B. Li, F. M. Wu, S. S. Li, and J. B. Xia, *J. Phys. Chem. C*, 2011, **115**, 20466.
  - 44 A. Bejan, and A. D. Allan, *Heat Transfer Handbook* (Wiley, New York), 2003, p1338.
  - 45 S. Siebentritt, R. Pues, K.-H. Rieder, and A. M. Shikin, *Phys. Rev. B*, 1997, **55**, 7927.
  - 46 J.-A. Yan, W. Y. Ruan, and M. Y. Chou, *Phys. Rev. B*, 2008, **77**, 125401.
  - 47 D. L. Nika, S. Ghosh, E. P. Pokatilov, and A. A. Balandin, *Appl. Phys. Lett.*, 2009, **94**, 203103.
  - 48 S. Ghosh, I. Calizo, D. Teweldebrhan, E. P. Pokatilov, D. L. Nika, A. A. Balandin, W. Bao, F. Miao and C. N. Lau, *Appl. Phys. Lett.*, 2008, **92**, 151911.
  - 49 K. Esfarjani, and G. Chen, *Phys. Rev. B*, 2011, **84**, 085204.
  - 50 J. Shiomi, K. Esfarjani, and G. Chen, *Phys. Rev. B*, 2011, **84**, 104302.